

## Supporting Information

### **One-Pot Two-Step Synthesis of Micro- and Mesoporous Organic Fibrils for Efficient Pseudocapacitors**

Minwoo Yang and Woon Ju Song\*

#### **Table of Contents**

<b>Materials .....</b>	<b>2</b>
<b>Synthesis and characterization of 1,4,5,8,9,12-hexaazatriphenylene hexacarboxylic acid ..</b>	<b>3</b>
<b>Synthesis of PI-Fiber .....</b>	<b>6</b>
<b>TEM and SEM images of PI-Fiber .....</b>	<b>7</b>
<b>FT-IR, <sup>13</sup>C NMR, XPS and TGA of PI-Fiber .....</b>	<b>13</b>
<b>PXRD and N<sub>2</sub> adsorption of PI-Fiber .....</b>	<b>16</b>
<b>Electrode fabrication and electrochemical properties in three- and two-electrode systems .....</b>	<b>19</b>
<b>References.....</b>	<b>32</b>

## Materials

Melamine, glyoxal, potassium hydroxide (KOH), sodium hydrogen carbonate ( $\text{NaHCO}_3$ ), sodium sulfite ( $\text{Na}_2\text{SO}_3$ ), diaminomaleonitrile, sodium nitrite ( $\text{NaNO}_2$ ), glacial acetic acid, mesitylene, isoquinoline, N-methyl-2-pyrrolidone (NMP), dimethylacetamide (DMAC), 1,3-dimethyl-2-imidazolidinone (DMI), dimethylsulfoxide (DMSO), graphitic foil, carbon black, and activated carbon were purchased from Thermo Fischer scientific. Concentrated hydrogen chloride (HCl), sulfuric acid ( $\text{H}_2\text{SO}_4$ ), trifluoroacetic acid, and activated charcoal were supplied from the DAEJUNG chemical. Ethyl alcohol (EtOH), methyl alcohol (MeOH), ethyl acetate (EA), dichloromethane (DCM), diethyl ether, acetone, and hexane were purchased from SAMCHUN chemical and DAEJUNG chemical in analytical grades. Silver nitrate ( $\text{AgNO}_3$ ) and tetrabutylammonium perchlorate ( $\text{NBu}_4\text{ClO}_4$ ) were supplied from Sigma-Aldrich. All chemicals were used without further purification unless noted.

Commercially available electrodes (Ag/Ag<sup>+</sup> reference electrode, Hg/HgO reference electrode, glassy carbon electrode) were provided by Qrins. Pt wires were purchased from 4science.net. All solutions used in electrochemical experiments were made in the laboratory and filtered through a 0.22  $\mu\text{m}$  size filter before usage.

## Synthesis and characterization of 1,4,5,8,9,12-hexaazatriphenylene hexacarboxylic acid (HATCO<sub>2</sub>H)

The synthesis of HATCO<sub>2</sub>H was according to previously published procedures with slight modifications.<sup>1-2</sup>

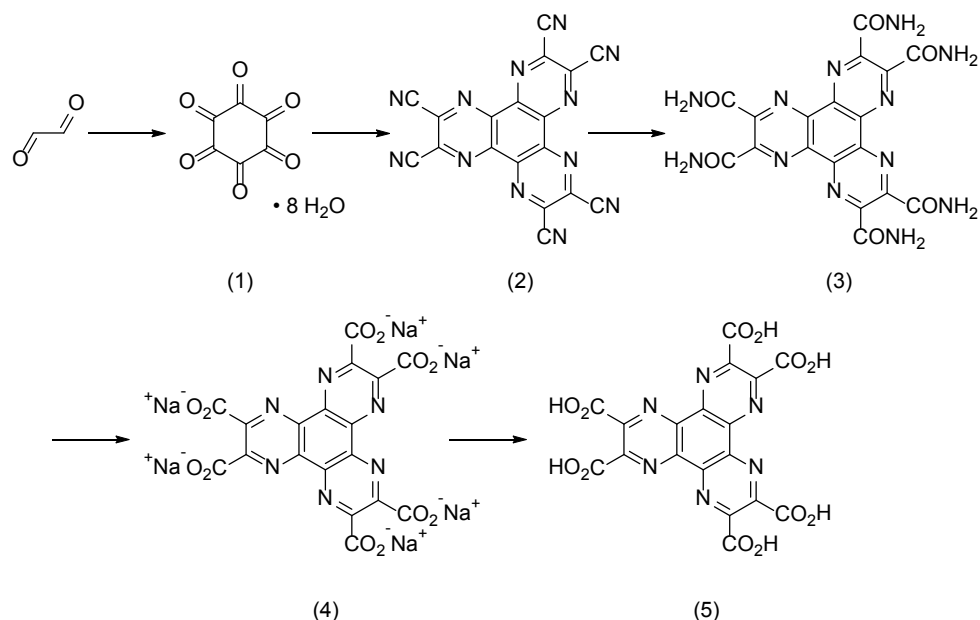


Fig. S1. Synthesis of 1,4,5,8,9,12-hexaazatriphenylene hexacarboxylic acid.

Synthesis of hexaketocyclohexane octahydrate (1) was carried out by following the previously reported procedure.<sup>3</sup> NaHCO<sub>3</sub> (60 g) and Na<sub>2</sub>SO<sub>3</sub> (160 g) dissolved in 1200 ml of ddH<sub>2</sub>O were heated to 40 °C. The solution described above was stirred and mixed with 192 ml of glyoxal while air bubbling. After 1 h stirring, the darkened suspension was heated to 90 °C at a rate of 1 °C min<sup>-1</sup>. Then, air bubbling stopped, and the resulting suspension was further incubated at 120 °C for 15 min, then cooled to room temperature. After overnight incubation, the dark suspension was filtered, and the resulting precipitant was washed with ddH<sub>2</sub>O and MeOH. After drying under air, the precipitant was added portionwise into 80 ml of 25 % aqueous HNO<sub>3</sub> solution at 0 °C. Further incubation at -20 °C resulted in the precipitation of white solid. After filtration, 6 g of the desired product was obtained.

The mixture of 5 g of (1) and 13 g of dicyanodiamine in 600 ml of glacial acetic acid was refluxed for 3 h. The resulting suspension was cooled to room temperature, filtered, and washed with acetic acid. Absolute drying under vacuum condition yielded 4.8 g of dark-colored precipitant (2), which was used without further purification.

A solution of 4.8 g of (2) in 150 ml of 98 % H<sub>2</sub>SO<sub>4</sub> was vigorously stirred for 3 d at room temperature. The suspension was then poured into 2 L of ice-cold ddH<sub>2</sub>O, then centrifuged at 5000 rpm. The pelletized sample was collected, washed with ddH<sub>2</sub>O, and dried at 100 °C to yield 6.2 g of (3) as gray-black solid.

To a stirring suspension of 6.2 g of (3) in 190 ml of trifluoroacetic acid, 8.8 g of NaNO<sub>2</sub> was added portionwise for 15 min at 0 °C. The reaction mixture turned to reddish color with gas generation. Glacial acetic acid (190 ml) was further added to the suspension, then stirred for 18 h at room temperature. The reaction mixture was treated with 370 ml of ddH<sub>2</sub>O, and the colloidal suspension was centrifuged at 5000 rpm. After removing the supernatant, the remaining solid was dissolved in aqueous NaHCO<sub>3</sub> solution (24 g in 180 ml ddH<sub>2</sub>O), and the resulting reddish suspension was filtered. The filtrate was treated with activated charcoal, heated to 100 °C, and stirred for 30 min. The mixture was then filtered, and the filtrate was added to NaOH solution (24 g in 120 ml ddH<sub>2</sub>O). After that, addition of 30 ml of EtOH to the cooled mixture precipitated light yellow colored solids, which was then filtered to yield 6.2 g of sodium salts of hexaazatriphenylene hexacarboxylate (4).

The aqueous suspension of sodium hexaazatriphenylene hexacarboxylate salts (5 g in 150 ml) were heated to 50 °C, acidified by adding 150 ml of concentrated HCl and stirred for 1 h at 90 °C. After cooling the solution, the crude mixture was filtered and washed with ddH<sub>2</sub>O to yield 3.7 g of HATCO<sub>2</sub>H (5) as a white powder.

The <sup>13</sup>C NMR spectra of HATCO<sub>2</sub>H was recorded on a Varian 500 (Varian), and the data are consistent with the previously reported values (Fig. S2).<sup>4</sup>

Liquid Chromatography Electrospray Ionization Mass Spectroscopy (LC-ESI-MS) spectra were recorded on 1260 Infinity LC/6120 Quadrupole LC-MS (Fig. S3); Calculated for C<sub>18</sub>H<sub>6</sub>N<sub>6</sub>O<sub>12</sub>, 498.27; Observed: [M + H]<sup>+</sup> = 499.0, [M + NH<sub>4</sub>]<sup>+</sup> = 516.0.

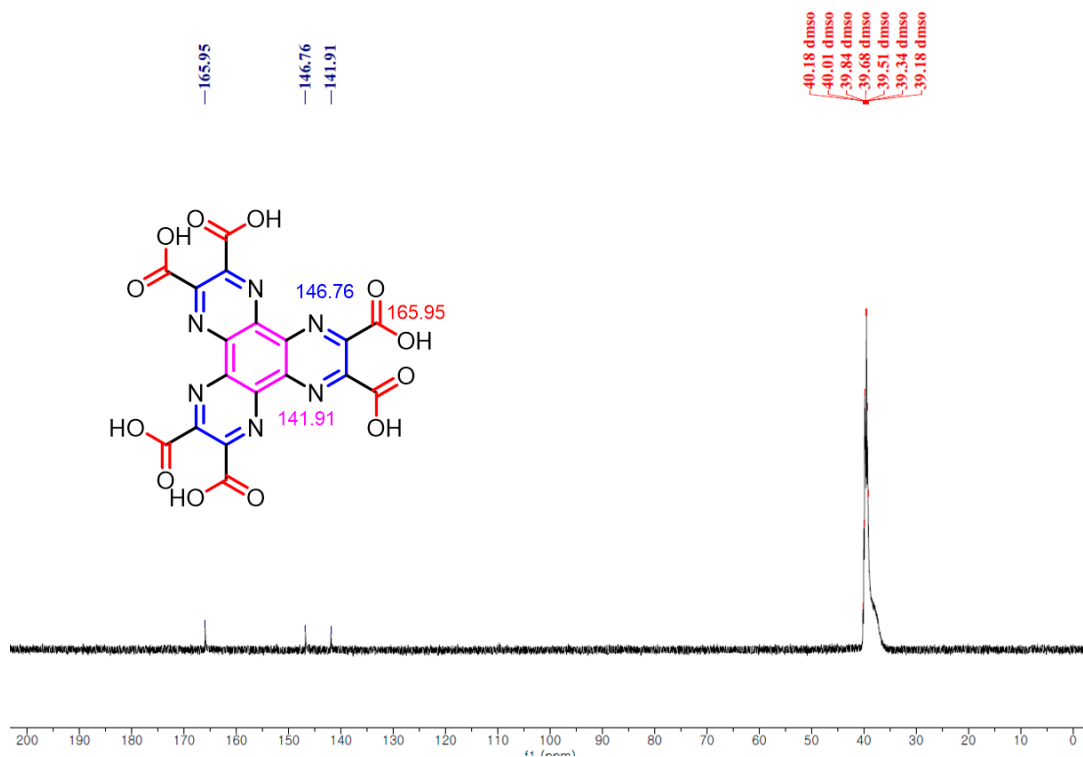


Fig. S2.  $^{13}\text{C}$  NMR spectrum of HATCO<sub>2</sub>H (500 MHz, [D<sub>6</sub>]DMSO):  $\delta$ =165.95 ppm (CO<sub>2</sub>H), 146.76 ppm (external Ar), 141.91 ppm (internal Ar).

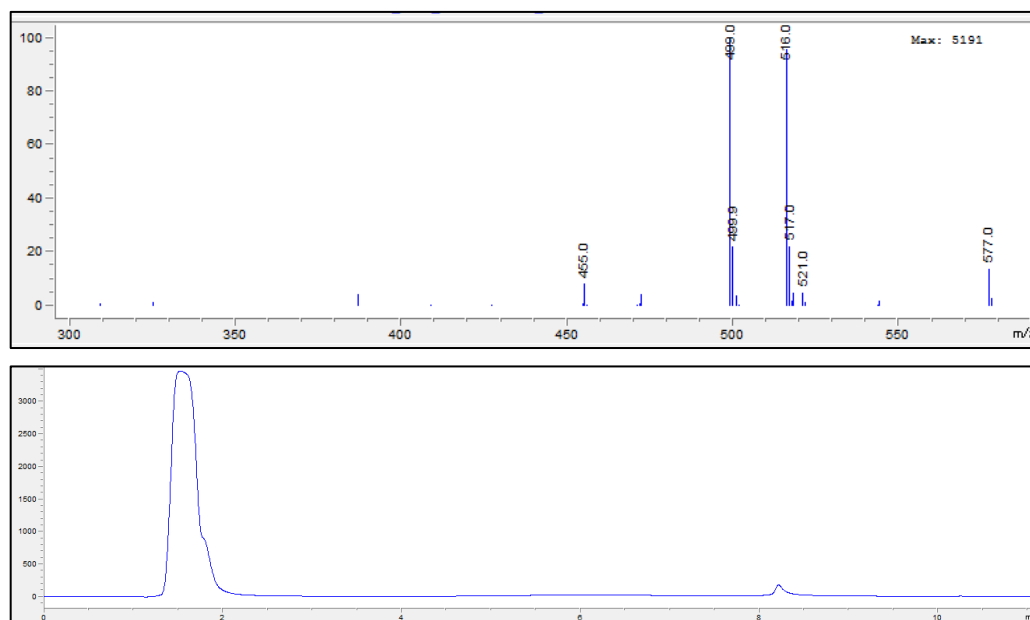


Fig. S3. Liquid chromatography and mass spectrometry spectrum of HATCO<sub>2</sub>H. MS (EI) m/z calculated for C<sub>18</sub>H<sub>6</sub>N<sub>6</sub>O<sub>12</sub>, 498.27 m/z (%): 498.0 (100), 499 (19.5), 500 (2.5). Observed: 499.0 (100), 499.9 (22.5), 500 (3.6) [M + H]<sup>+</sup>, 516.0 (100), 517.0 (22.5), 518 (2.6) [M + NH<sub>4</sub>]<sup>+</sup>.

### **Synthesis of PI-Fiber**

The mixture of HATCO<sub>2</sub>H (100 mg) and melamine (25.2 mg) in 16 ml of anhydrous N-methyl-2-pyrrolidone (NMP) was vigorously stirred for 24 h at 75 °C under Ar. Pale yellow precipitant was initially formed and slowly solubilized to form a dark-colored solution as shown in Fig. 1c. After the addition of 1 ml of mesitylene and isoquinoline, the resulting solution was incubated for 2–3 days at 200 °C. After filtration, washing with NMP, ethanol, dichloromethane, acetone, ethyl acetate, hexane, and methanol, and drying under vacuum at 200 °C, dark-colored solids (**PI-Fiber**) were isolated (46.3 mg, 37 %).

### **TEM and SEM images of PI-Fiber**

Carbon-coated 200-mesh copper grids (CF200-Cu) were purchased from Electron Microscopy Sciences and were directly applied to sample preparation without any treatment. TEM was operated at HITACHI H-7600 (HITACHI-Science & technology, 120 kV), using AMTV542 software. Field effect scanning electron microscopy (FE-SEM) and energy dispersive X-ray spectroscopy (EDS) images were acquired using HSM-6700F (JEOL Ltd, Japan) installed at the national center for inter-university research facilities (NCIRF) at Seoul national university (SNU) at an accelerating voltage of 5 kV. Before each measurement, samples loaded onto carbon tapes were sprayed by the platinum ion beam.

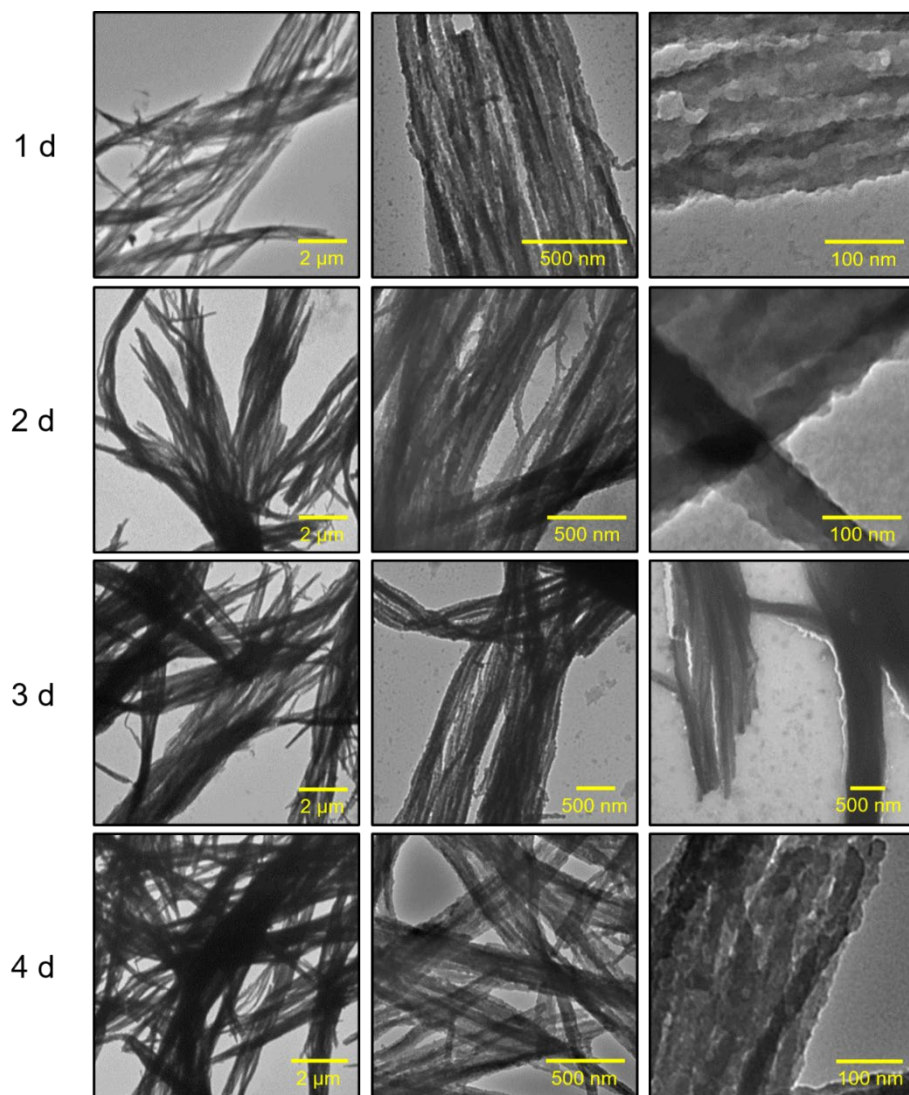


Fig. S4. Time-dependent TEM images of samples during imidization.

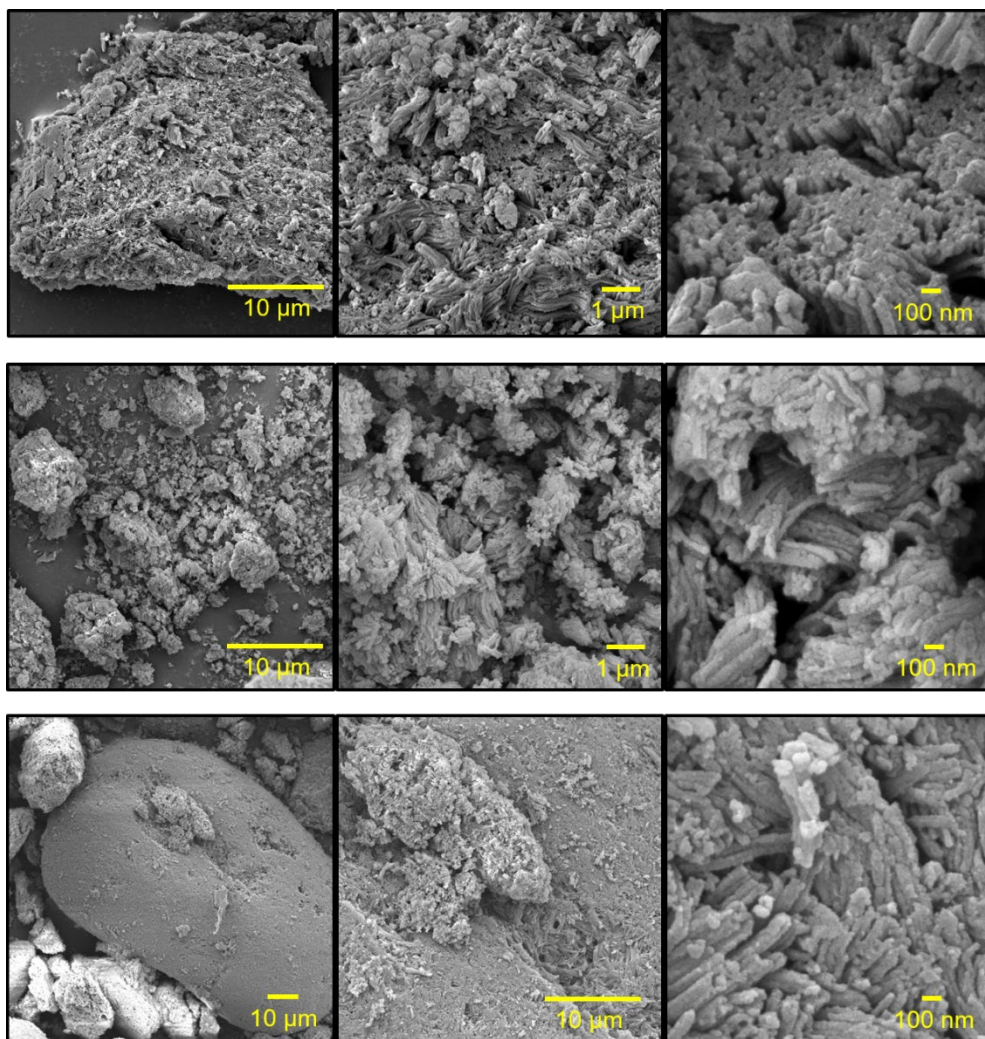


Fig. S5. SEM images of PI-Fiber. All images show fibril structures with some variations in overall morphology and size.

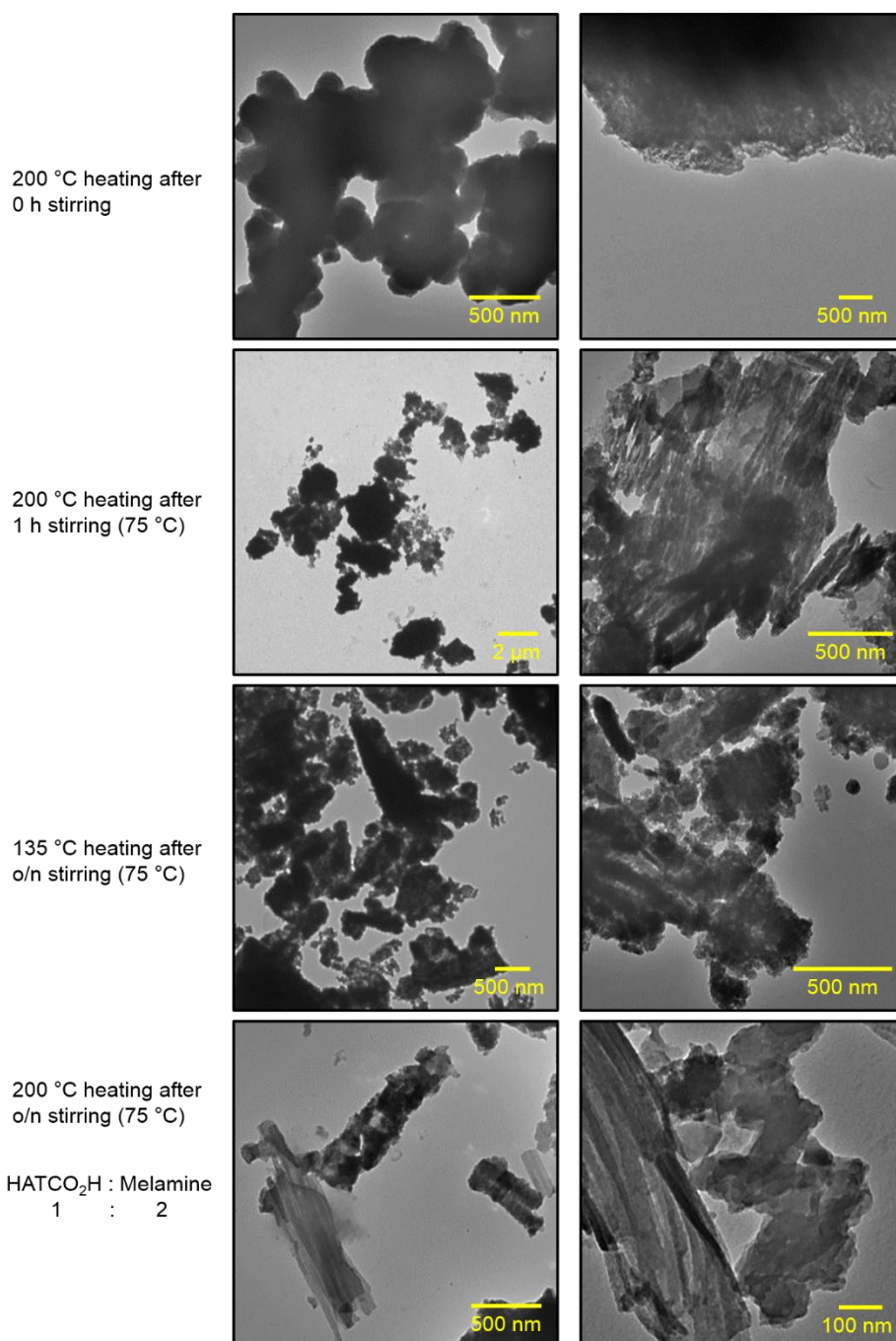


Fig. S6. TEM images of samples prepared under unoptimized conditions. The modification of temperature for imidization, incubation time for pre-assembly, or the ratio of two monomers, as described on the left, led to heterogeneous or partially fibril structures.

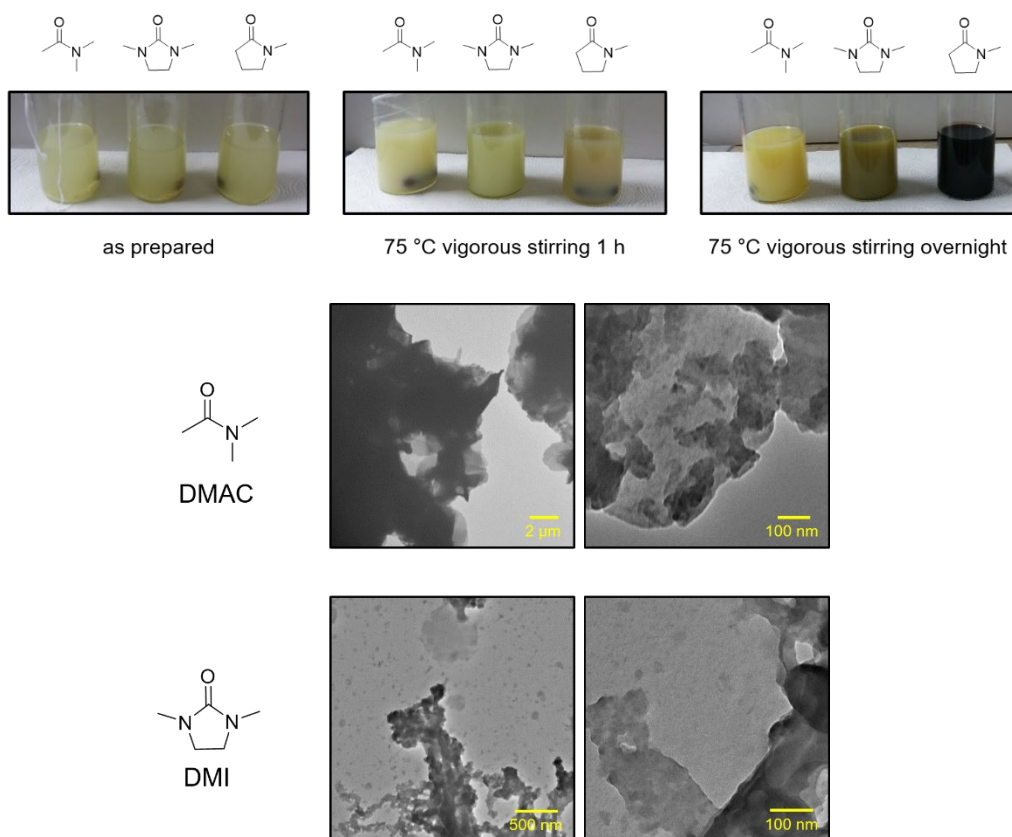


Fig. S7. TEM images of samples synthesized in solvents other than NMP. HATCO<sub>2</sub>H (100 mg) and melamine (25.2 mg) in 16 ml of each solvent (DMAC or DMI) were mixed. They failed to solubilize pre-assembled monomers, resulting in the formation of heterogeneous precipitants after imidization.

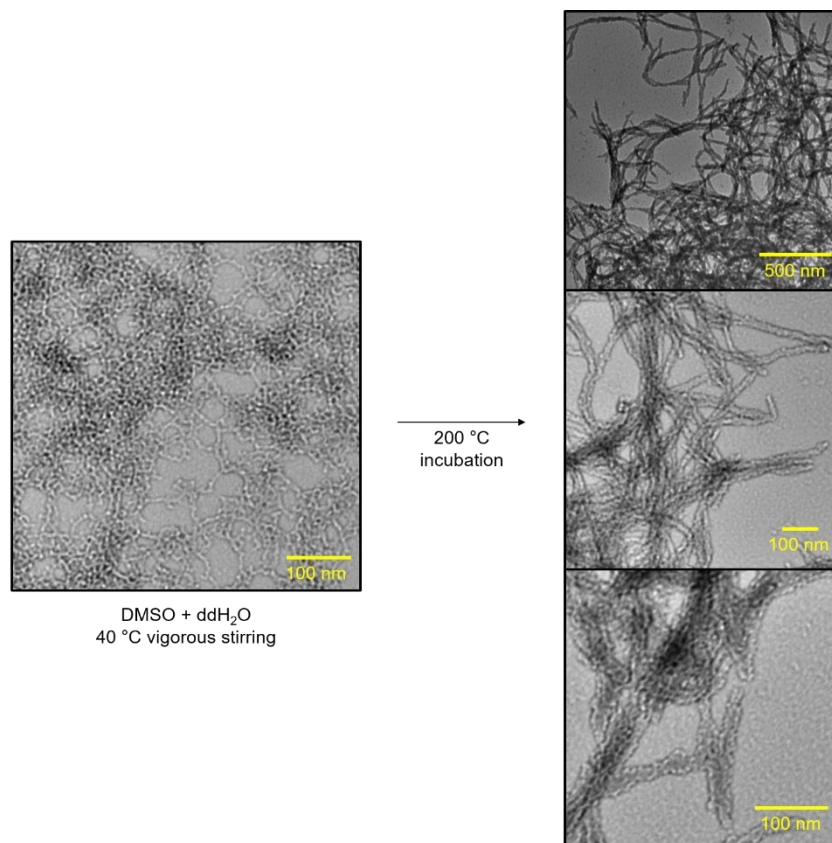


Fig. S8. TEM images of pre-assembled and imidized samples in DMSO solvent. HATCO<sub>2</sub>H (100 mg) and melamine (25.2 mg) were dissolved in 16 ml of DMSO with 40  $\mu$ L of ddH<sub>2</sub>O for the subsequent reactions.

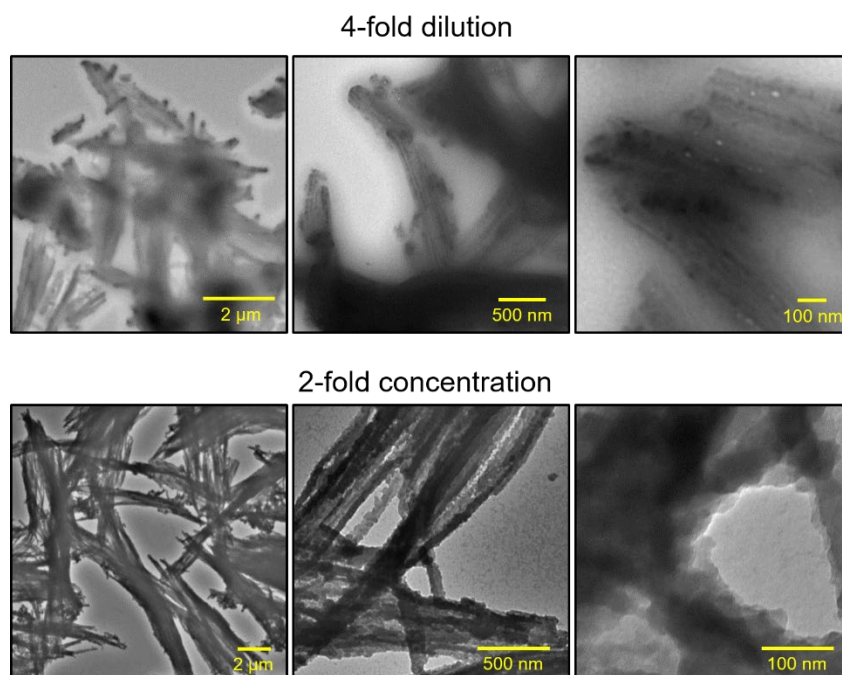


Fig. S9. TEM images of fibrils synthesized with various concentrations of monomers. Either 4-fold diluted (25 mg of HATCO<sub>2</sub>H and 6.3 mg of melamine) or 2-fold concentrated (200 mg of HATCO<sub>2</sub>H and 50.4 mg of melamine) monomers were reacted in 16 ml NMP.

### **FT-IR, <sup>13</sup>C NMR, XPS and TGA of PI-Fiber**

Fourier Transform Infrared (FT-IR) experiments were conducted using Spectrum Two (PerkinElmer) in reflection mode in the range of 600–4000 cm<sup>-1</sup>.

Solid-State <sup>13</sup>C cross-polarization magic angle spinning/total suppression of spinning sidebands (CP-MAS/TOSS) NMR spectra were acquired between -20 ppm and 240 ppm using 500 MHz Bruker Avance III HD (Bruker, German) installed at NCIRF at SNU at the spinning rate of 5 kHz.

The C, H, N element ratio was analyzed by Micro CHNS (TruSpec) installed at SNU chemical & biological engineering research facilities.

X-ray photoelectron spectroscopy (XPS) was conducted by screening pelletized samples using AXIS SUPRA (Kratos, UK) installed at NCIRF at SNU at a base pressure under 5×10<sup>-8</sup> Pa.

The thermal stability of samples was examined using Discovery TGA (TA Instruments, USA) installed at the national instrumentation center for environmental management (NICEM) at SNU. Temperature between 25 °C and 800 °C was applied at the heating rate of 10 °C min<sup>-1</sup> under dinitrogen conditions.

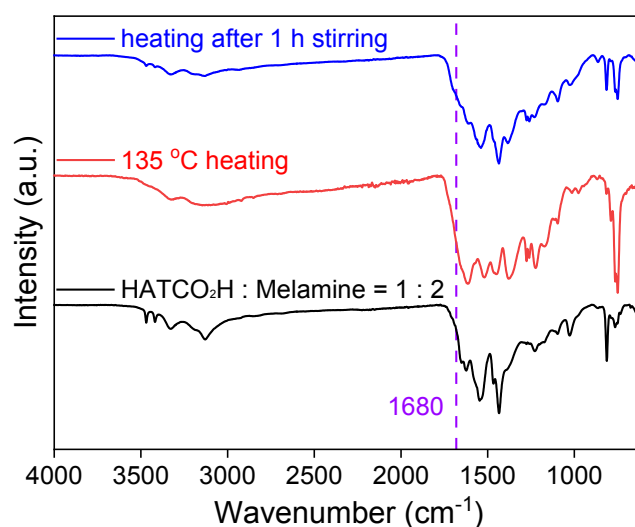


Fig. S10. FT-IR spectrum of samples generated from the conditions in Fig. S6. Broad peaks around 3000–3500  $\text{cm}^{-1}$ , negatively-shifted carbonyl peaks at 1650  $\text{cm}^{-1}$ , and absence at 1680  $\text{cm}^{-1}$  indicate incompletely reacted polyamic acid due to incomplete imidization of two monomers.

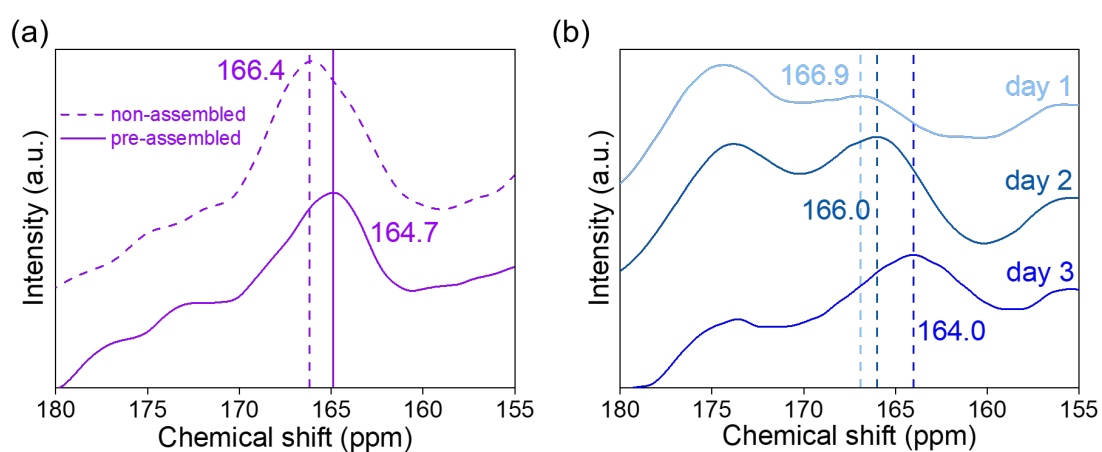


Fig. S11. The carbonyl region of  $^{13}\text{C}$  ssNMR spectra. (a) The imidized products without pre-assembly (non-assembled) versus pre-assembled PI-Fiber. (b) The time-dependent spectrum of PI-fiber formation for 1–3 days.

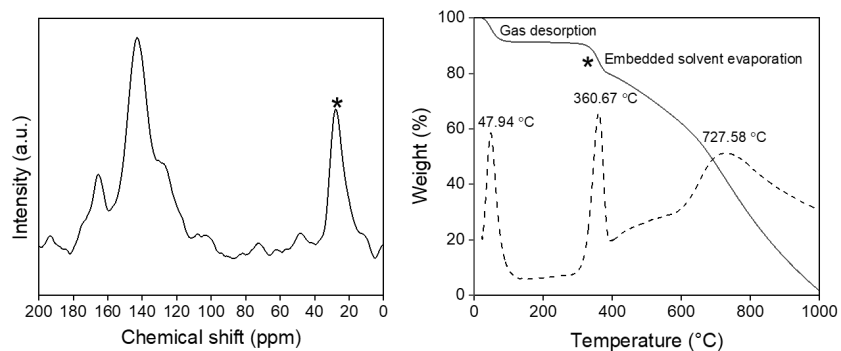


Fig. S12. (a) The  $^{13}\text{C}$  NMR spectrum and (b) TGA curves of PI-Fiber. The residual NMP solvent shown in both spectra is denoted as asterisks.

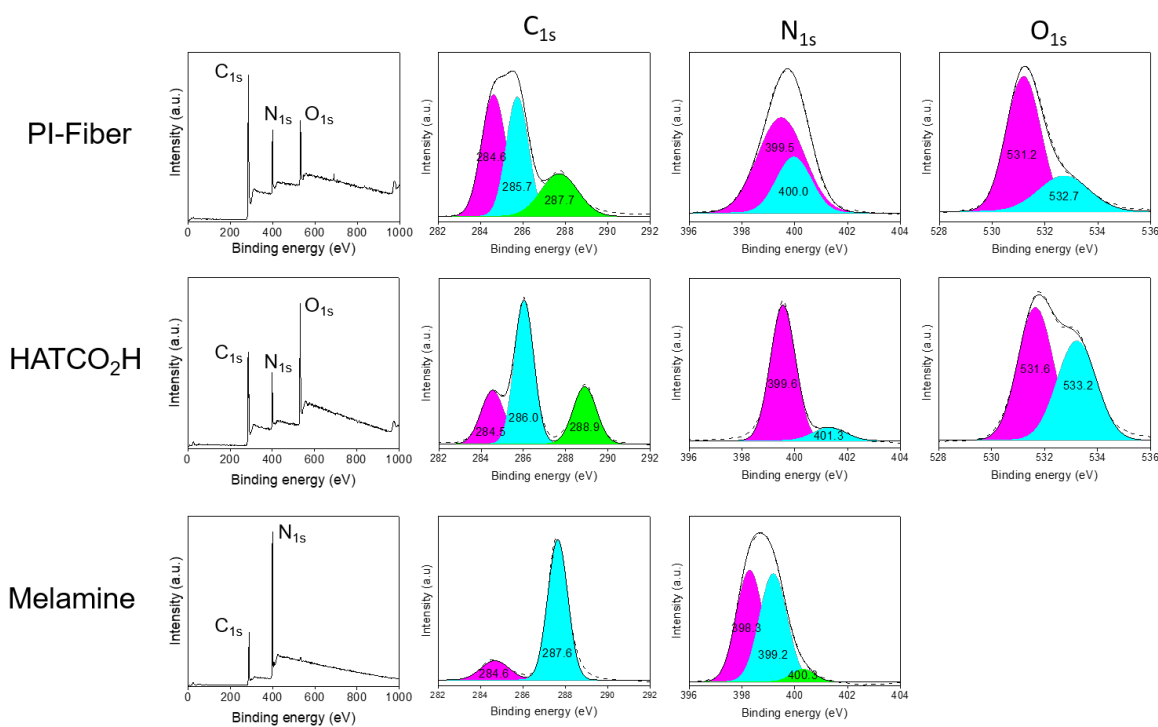


Fig. S13. XPS spectrum of PI-Fiber, HATCO<sub>2</sub>H, and melamine. Full spectrum and high-resolution profile of  $\text{C}_{1s}$ ,  $\text{N}_{1s}$ , and  $\text{O}_{1s}$  are represented.

### **PXRD and N<sub>2</sub> adsorption of PI-Fiber**

Powder X-ray Diffraction (PXRD) patterns were measured using SmartLab (Rigaku) installed in NCIRF at SNU with a 3kW of X-ray generator (Cu target) and D/teX Ultra250 detector. The pore structure of PI-Fiber calculated from Density Functional Theory (DFT) was determined by Accelrys Materials Studio 8.0 software package. DFT calculation for geometry optimization was conducted by using GGA PBE (General Gradient Approximation applying Perdew-Burke-Ernzerhof) functional with Dmol3 tools. The simulated structures of AA and AB stacking models were acquired from Castep tools in Accelrys Materials Studio 8.0 software package. Castep geometry optimization with fixed basis quality was carried out using GGA PBE function.

Brunauer-Emmett-Teller surface area and micropore size analysis were measured from N<sub>2</sub> adsorption-desorption kinetics conducted at 77 K by Micromeritics (3Flex) installed at KAIST analysis center for research advancement (KARA). The pore size distribution was calculated from the nonlocal density functional theory (NLDFT) method. The samples were degassed at 200 °C for more than 8 h under vacuum.

High-resolution transmission electron microscopy (HR-TEM) images were acquired using JEM-3010 (HEOL Ltd, Japan) installed at NCIRF at SNU with an acceleration electron voltage of 300 kV.

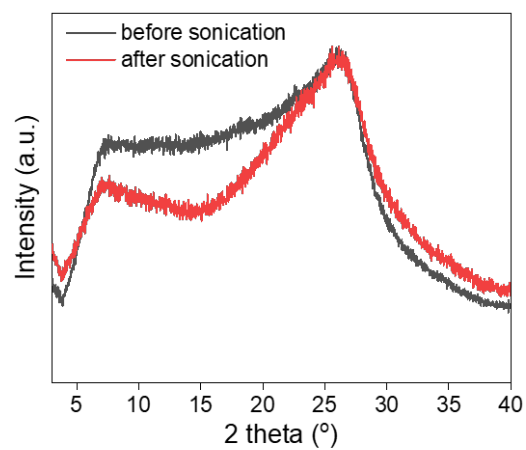


Fig. S14. The PXRD patterns of PI-Fiber. The signals were slightly improved after sonication.

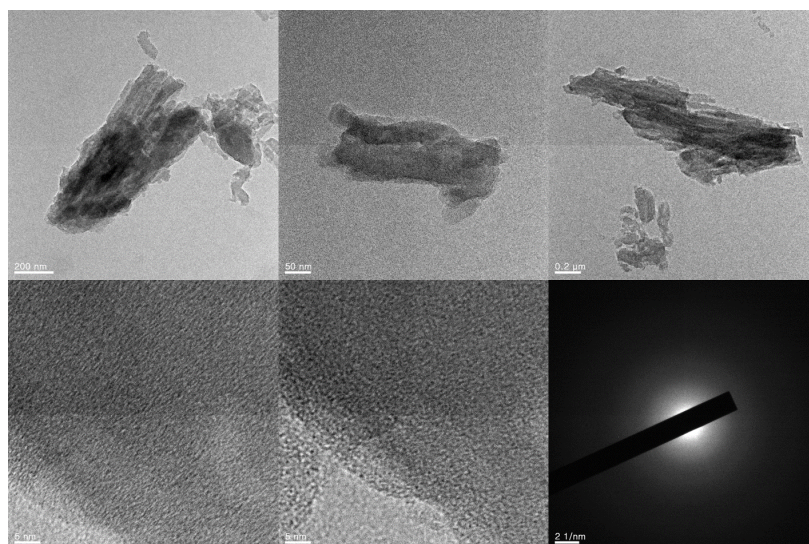


Fig. S15. HR-TEM images of PI-Fiber. No discrete crystallinity was observed as shown in PXRD data.

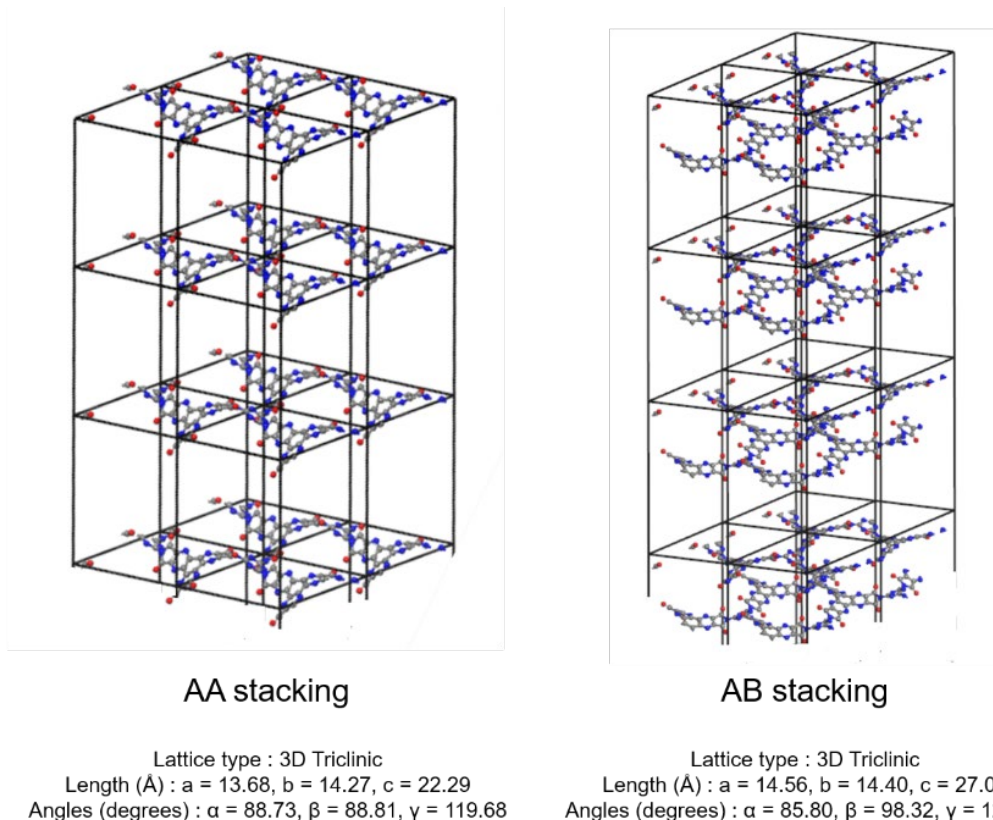


Fig. S16. Simulated structures of AA stacking and AB stacking models (grey: carbon, blue: nitrogen, and red: oxygen). The lattice parameter of each model is indicated below. Both structures show desymmetrized (100) and (010) facets and extended layer-layer distance along with z-axis due to the innate distorted shape of the building block.

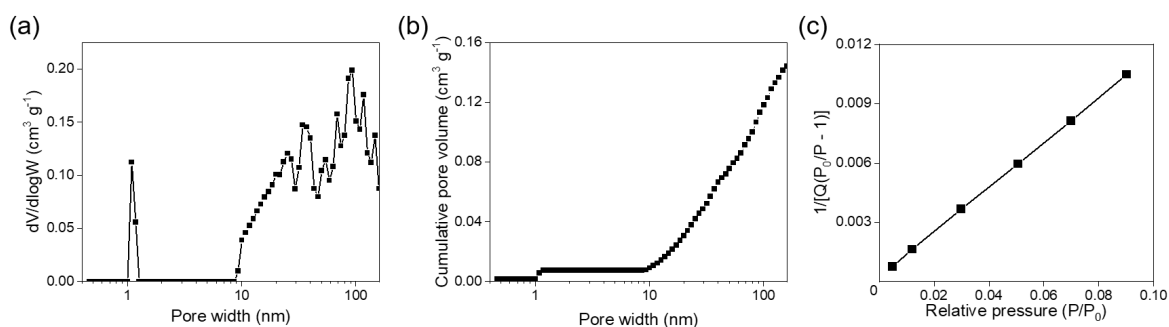


Fig. S17. Plots acquired from  $\text{N}_2$  adsorption and desorption isotherm at 77 K. (a) Incremental and (b) Cumulative pore volume. (c) Multi-point BET plot.

### **Electrode fabrication and electrochemical properties in three- and two-electrode systems**

Cyclic voltammetry and galvanostatic charge and discharge measurements were performed using Autolab PGSTAT101 and were analyzed with a NOVA software. Three electrode-setup was assembled using the hand-made graphitic foil electrode as a working electrode, Pt wire or hand-made activated carbon electrode as a counter electrode, and Hg/HgO electrode in 20 % (w/v) aqueous KOH solution as a reference electrode. Electrochemical experiments were conducted under argon atmosphere.

Hand-made graphite foil electrodes were prepared as follows; 3 mg of the mixture containing active material, carbon black, and polyvinylidene fluoride was suspended in 0.6 ml of NMP and sonicated. The resulting slurry was then drop cast onto graphitic foil and dried overnight at room temperature. 0.5 mg of sample in total was loaded, and the rest of the electrode surface was sealed with adhesives (Loctite@Hankel).

Electrochemical impedance spectroscopy was carried out with VSP-300 potentiostat (BioLogic). The Nyquist diagram was plotted against the indicated offset voltage in the frequency range of 10 kHz and 20 mHz with a sinus amplitude of 10 mV.

The asymmetric two-electrode cell was made using the working electrode described above as a negative electrode and an activated carbon electrode as a positive electrode in aqueous 6 m KOH solution.

We calculated HOMO, LUMO levels of PI-Fiber by using  $E_{\text{oxi, onset}}$ ,  $E_{\text{red, onset}}$  values of PI-Fiber and  $E_{1/2}$  value of ferrocene (0.09 V vs Ag/Ag<sup>+</sup>) at the same conditions. Onset potentials were acquired by estimating the intersection between the base line and tangent at the highest of the slope ( $E_{\text{oxi, onset}} = 0.89$  V vs Ag/Ag<sup>+</sup>,  $E_{\text{red, onset}} = -0.72$  V vs Ag/Ag<sup>+</sup>). HOMO and LUMO levels vs vacuum were calculated by following equations;<sup>5</sup>

$$E_{\text{LUMO}}(\text{eV}) = -[E_{\text{red, onset}} - E_{1/2}(\text{ferrocene}) + 4.8]$$

$$E_{\text{HOMO}}(\text{eV}) = -[E_{\text{oxi, onset}} - E_{1/2}(\text{ferrocene}) + 4.8]$$

The current densities ( $I$ ) were calculated by dividing current ( $i$ ) into the loaded mass of active materials ( $m_a$ );  $I \text{ (A g}^{-1}\text{)} = \frac{i}{m_a}$

The charge capacities from cyclic voltammetry curves were calculated by integrating CV curves (A) and using the following equation, where  $v$  indicates scan rate;

$$Q \text{ (C g}^{-1}\text{)} = \frac{A}{2m_a v}$$

The charge capacities from galvanostatic charge and discharge experiments were calculated by multiplying the applied current density,  $I \text{ (A g}^{-1}\text{)}$ , with discharging time,  $t \text{ (s)}$ ,

$$Q \text{ (C g}^{-1}\text{)} = I \times t$$

Specific energy densities ( $E$ ) and power densities ( $P$ ) from two electrode charge-discharge experiments were calculated from the following equations,

$$E = I \int_0^t V dt, P = \frac{E}{t}$$

Coulombic efficiencies were calculated by dividing discharging time by charging time from galvanostatic experiments. All charge capacity values were reported as  $\text{mAh g}^{-1}$ .

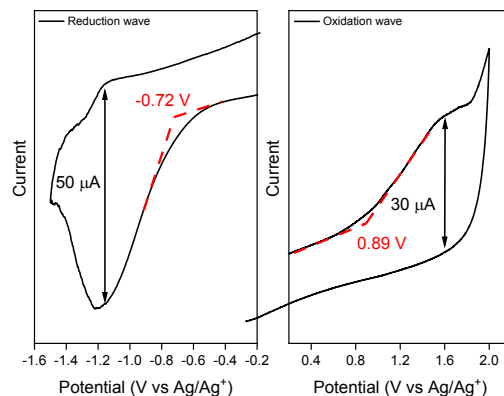


Fig. S18. The cyclic voltammograms of PI-Fiber. The slurry mixture of active materials, carbon black, and PVDF in ACN was deposited onto a glassy carbon electrode, and was used as working electrode. Pt wire and Ag/Ag<sup>+</sup> electrode (10 mM AgNO<sub>3</sub>) were used as counter and reference electrodes, respectively. As electrolytes, 100 mM NBu<sub>4</sub>ClO<sub>4</sub> was used in ACN.

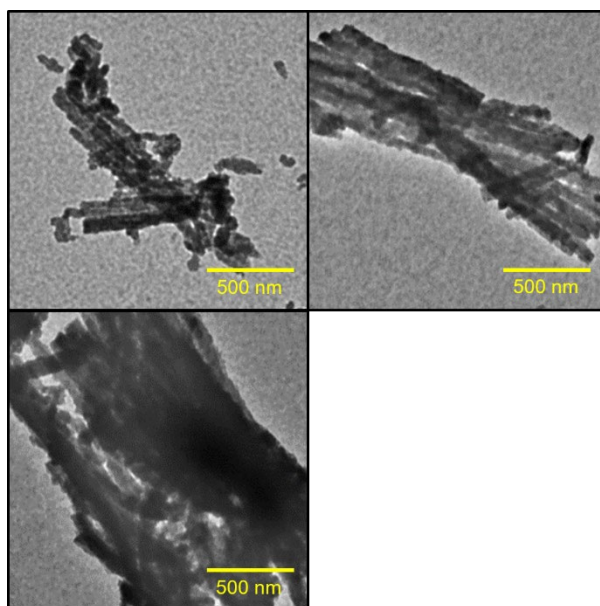


Fig. S19. TEM images of fragmented fibrils by sonication. PI-Fiber (< 1 mg) in 4 ml of NMP were sonicated for 2 h, and shortening and fragmentation was observed while maintaining the overall morphology.

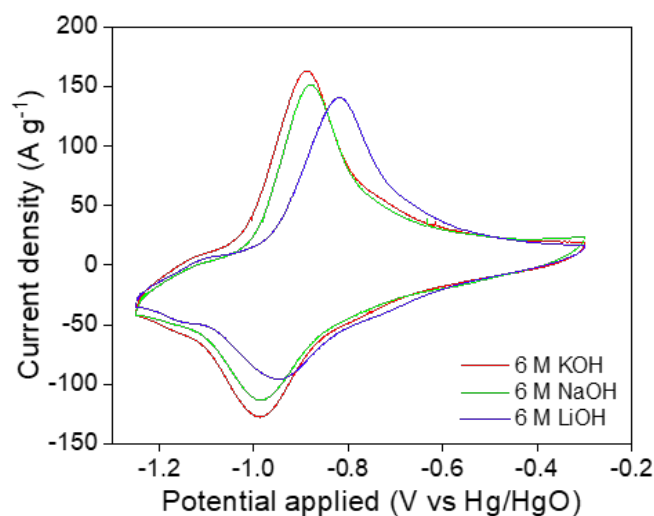


Fig. S20. CV curves measured at 100 mV s<sup>-1</sup> in various electrolytes. All three curves were measured from the same electrode in the order from KOH to LiOH. To avoid any complexity and experimental errors associated with the preparation of electrode, we re-used the electrode after washing and incubation for 1 h in the solution with electrolytes of our interest prior to the next measurements.

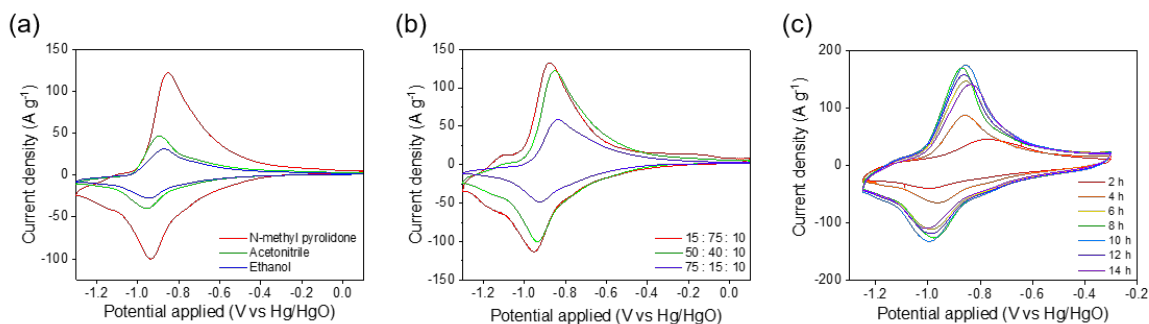


Fig. S21. CV curves of working electrodes prepared by sonication under various conditions. (a) Solvent effects. The slurry mixture of active materials, carbon black, and PVDF was sonicated for 4–5 h in the specified solvents. (b) The various ratio of the active materials, carbon black, and PVDF. Sonication was conducted in NMP solvent for 4–5 h. The high fraction of the active materials up to 75% reduced charge capacity presumably due to low conductivity of PI-Fiber. Thus, the ratio of 50: 40: 10 was selected as the optimal condition for further measurements. (c) Sonication time. The highest current density was observed after 8–10 h of sonication. All curves were acquired at 100 mV s<sup>-1</sup>.

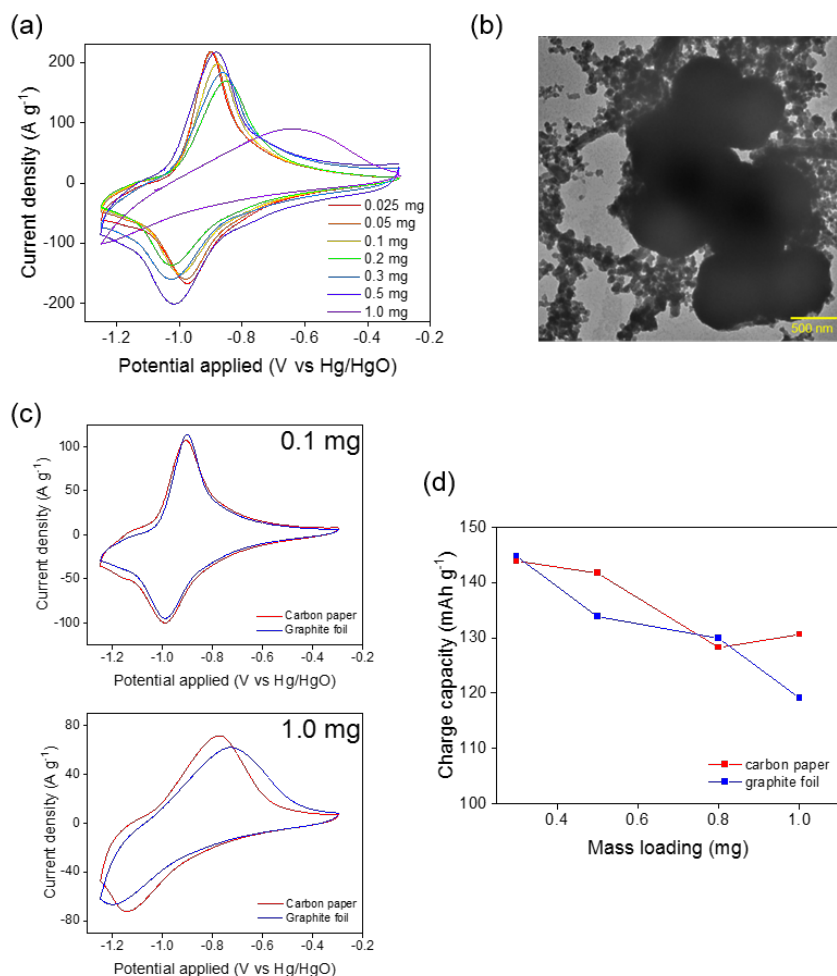


Fig. S22. Mass loading optimization. The mixture of active materials, carbon black, PVDF at the ratio of 50: 40: 10 was sonicated in NMP for 8–9 h before loading. (a) CV curves measured at  $100 \text{ mV s}^{-1}$  in the variation of the loaded amounts of the mixtures. The shape of curves and charge capacity retained analogously up to 0.5 mg of loading, but not with 1.0 mg of loading. (b) TEM image of the agglomerated species. (c) The overlaid CV curves recorded with carbon paper (red) or graphite foil (blue) as the substrate. The measurements were conducted at the sweep rate of  $50 \text{ mV s}^{-1}$ . (top) When 0.1 mg of the samples were loaded, no distinct change was observed. (bottom) With 1.0 mg of loading, significant changes in reversibility and charge capacity were observed with graphite foil, but not with carbon paper. The relatively reversible and high charge capacity with carbon paper might be associated with the high surface area and morphology of carbon paper. (d) Charge capacity against various mass loading and the substrates.

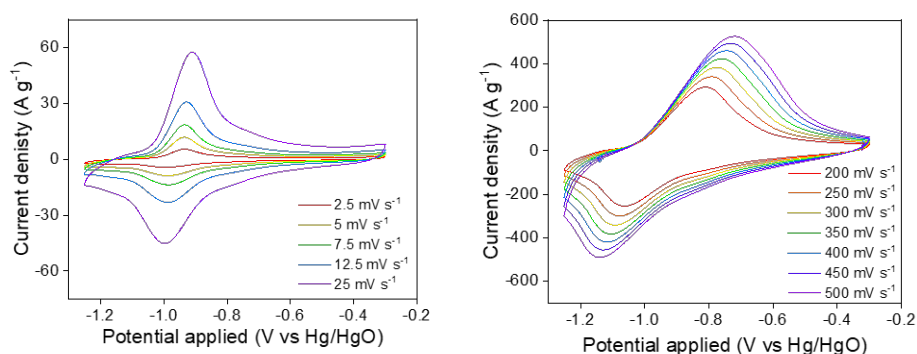


Fig. S23. CV curves of working electrodes in a three-electrode system (6 M KOH) at different sweep rates. The curves were measured at the rates of 2.5–500  $\text{mV s}^{-1}$ , and only the representative data are shown in Fig. 4c for clarity. Although the peak shift (V) increased with the faster sweep rates, a distinctive redox couple was observed even at the rate of 500  $\text{mV s}^{-1}$ .

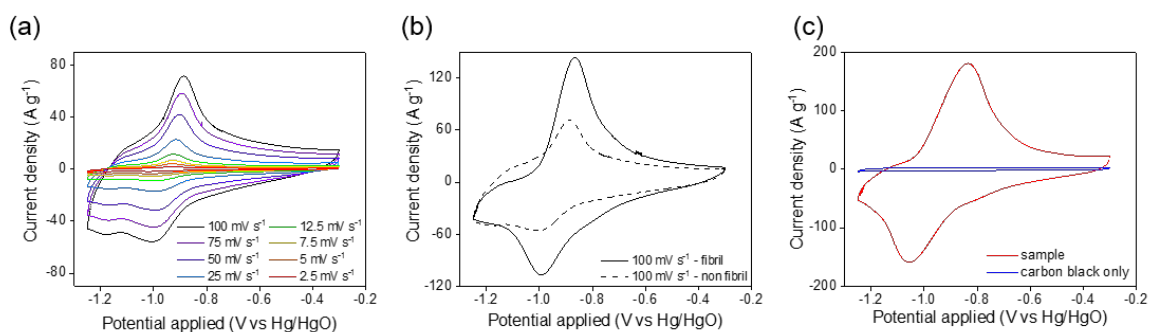


Fig. S24. Comparison of CV curves between fibrous and non-fibrous species. (a) CV curves of non-fibril samples in various sweep rates (2.5–100  $\text{mV s}^{-1}$ ). (b) The overlaid CV curves with fibril or non-fibril samples after cycling at the sweep rate of 100  $\text{mV s}^{-1}$ . These samples were cycled 500 times in the range of -0.1 V and -1.1 V vs Hg/HgO before the CV measurements. (c) CV curves of fibril and carbon black only loaded on the graphitic foil.

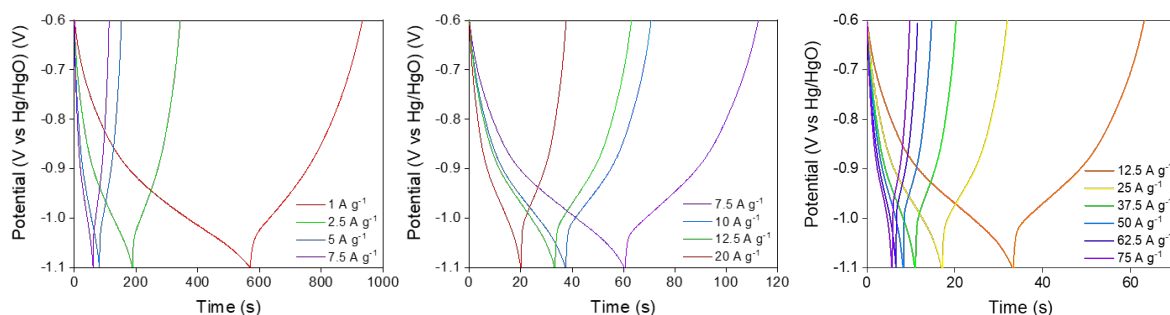


Fig. S25. GCD curves at various current densities (1–75  $\text{A g}^{-1}$ ).

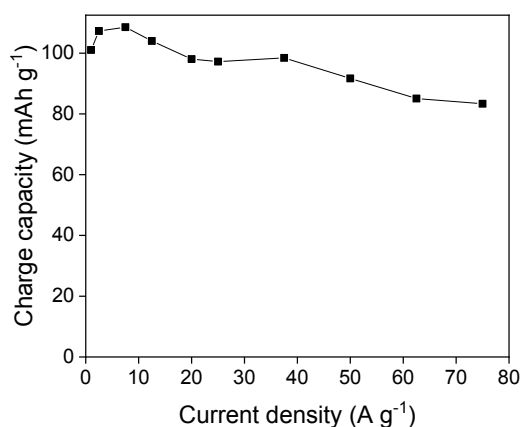


Fig. S26. A plot of charge capacity against current density using a freshly-prepared electrode with PI-Fiber. The charge was stored over 0.5 V range from -1.1 V to -0.6 V vs Hg/HgO. Even at high current density, decrease only less than 25% in charge capacity was observed.

Current density (A g <sup>-1</sup> )	Specific capacity (mAh g <sup>-1</sup> )	Columbic efficiency (%)
1	101.0	63.8
2.5	107.3	82.0
7.5	108.5	85.8
12.5	104.0	89.8
20	98.1	87.6
25	97.2	81.4
37.5	98.4	85.9
50	91.7	79.5
62.5	85.1	74.2
75	83.3	70.2

Table S1. Specific capacities and columbic efficiencies at different current densities.

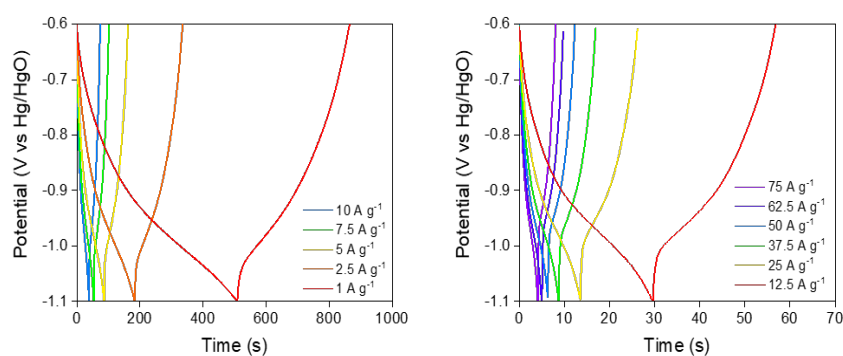


Fig. S27. GCD curves of the cycled electrode at different current densities (1–75 A g<sup>-1</sup>).

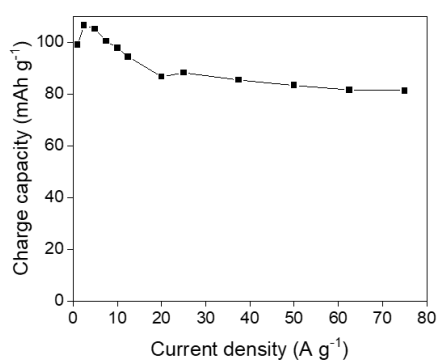


Fig. S28. Charge capacity (mAh g<sup>-1</sup>) of the cycled electrode stored over 0.5 V (-1.1 V – -0.6 V vs Hg/HgO) at different current densities (1–75 A g<sup>-1</sup>). Even at high current density, no drastic decrease in charge capacity was observed.

Current density (A g <sup>-1</sup> )	Specific capacity (mAh g <sup>-1</sup> )	Columbic efficiency (%)
1	99.0	70.2
2.5	106.5	84.2
5	105.1	87.5
7.5	100.4	90.3
10	97.8	91.4
12.5	94.4	91.9
20	86.7	93.4
25	88.2	94.1
37.5	85.4	94.3
50	83.3	95.2
62.5	81.6	94.0
75	81.3	95.1

Table S2. Specific capacities and columbic efficiencies of the cycled electrode at different current densities.

Species	Current density (A g <sup>-1</sup> )	Applied potential (voltage range)	Electrolyte	Charge capacity (mAh g <sup>-1</sup> )	Capacitance (F g <sup>-1</sup> )	Reference
PI-Fiber (Freshly-prepared)	2.5	-1.1 V ~ -0.6 V (vs Hg/HgO) (0.5 V)	6.0 M KOH	107.3	773	This work
	20			98.1	706	
	75			83.3	600	
	2.5			106.5	737	
	20			86.7	624	
	75			81.3	585	
AAM-TPB	1	0.2 V ~ 0.9 V (vs Ag/AgCl) (0.7 V)	1.0 M H <sub>2</sub> SO <sub>4</sub>	52.7	271	6
CNT/NKCOF-2	0.5	-0.1 V ~ 1.0 V (vs Ag/AgCl) (1.1 V)	2.0 M H <sub>2</sub> SO <sub>4</sub>	134.4	440	7
	20			66	216	
CNT/NKCOF-8	1	-0.2 V ~ 0.9 V (vs Ag/AgCl) (1.1 V)		72.7	238	
	20			45.8	150	
PHATN	0.5	-1.1 V ~ -0.6 V (vs Hg/HgO) (0.5 V)	6.0 M KOH	95.7	689	8
	20			80.1	577	
	75			60	432	
4KT-TpCOF	0.2	0 V ~ 0.6 V (vs Ag/AgCl) (0.6 V)	1.0 M H <sub>2</sub> SO <sub>4</sub>	97.2	583	9
	1			45.7	274	
	10			25.3	152	
TPT-DAHQ COF	0.5	-1.0 V ~ -0.1 V (vs Ag/AgCl) (0.9 V)	1.0 M KOH	78.2	313	10
	20			40	160	
Porous-1	0.2	-0.85 V ~ -0.35 V (vs Ag/AgCl) (0.5 V)	1.0 M Na <sub>2</sub> SO <sub>4</sub>	49	353	11
	1			29.7	214	
	10			10	72	
Porous-2	0.2	-0.9 V ~ -0.45 V (vs Ag/AgCl) (0.45 V)		29.8	238	
	1			26.6	213	
	10			17.3	138	
TaPa-(OH) <sub>2</sub>	0.5	-0.2 V ~ 0.5 V (vs SCE) (0.7 V)	1.0 M Phosphate	80.9	416	12
TPDA-1	0.5	0 V ~ 1.0 V (vs SCE) (1.0 V)	1.0 M H <sub>2</sub> SO <sub>4</sub>	96.7	348	13
	5			48.6	175	
TDFP-1	0.5	-0.5 V ~ 0.5 V (vs SCE) (1.0 V)	0.1 M H <sub>2</sub> SO <sub>4</sub>	116.1	418	14
DAAQ-TFP-COF	0.1	-0.3 V ~ 0.3 V (vs Ag/AgCl) (0.6 V)	1.0 M H <sub>2</sub> SO <sub>4</sub>	8	48	15
N-MPC	0.5	-1.0 V ~ 0 V (vs SCE) (1.0 V)	6.0 M KOH	140.3	505	16
	1			58.6	211	
	10			28.1	101	
HM-COF	0.5	0 V ~ 0.5 V (vs SCE) (0.5 V)	6.0 M KOH	20.1	145	17
	10			9.7	70	
POF-800	0.25	-1.0 V ~ -0.1 V (vs Ag/AgCl) (0.9 V)	6.0 M KOH	12.5	50	18
	10			2.8	11	
CPP	1	0 V ~ 0.45 V (vs Hg/HgO) (0.45)	6.0 M KOH	71.4	571	19
	10			39.6	317	
	1			39.5	316	
c-CNT@COF	0.2	-0.3 V ~ 0.3 V (vs Ag/AgCl) (0.6 V)	0.5 M H <sub>2</sub> SO <sub>4</sub>	69.8	419	20
	0.5			62.7	376	
BIBDZ	0.5	0 V ~ 1.0 V (vs SCE) (1.0 V)	1.0 M H <sub>3</sub> PO <sub>4</sub>	24.6	89	21
	10			11.9	43	

BPY-CTF				109.3	393	
CTF-1	0.5	-1.0 V ~ 0 V (vs Hg/HgO) (1.0 V)	1.0 M KOH	61.2	220	22
DCE-CTF				77.8	280	
DCP-CTF				90.1	324	
PyrOxin POP	1 5 10	0 V ~ 0.45 V (vs Hg/HgO) (0.45 V)	6.0 M KOH	65.2	522	23
				52.6	421	
				42.8	342	
An-CPOP-1	0.5	-1.0 V ~ 0.5 V (vs Hg/HgO) (1.5 V)	1.0 M KOH	30.1	73	24
An-CPOP-2				41	98	
TFP-NDA-COF	0.5	0 V ~ 1.0 V (vs SCE) (1.0 V)	1.0 M H <sub>2</sub> SO <sub>4</sub>	96.7	348	25
FCTF	1 5 10	0 V ~ 0.8 V (vs Ag/AgCl) (0.8 V)	1.0 M H <sub>2</sub> SO <sub>4</sub>	70.9	319	26
				66.7	300	
				58.4	263	
PPrGO-2	3	-0.2 V ~ 0.6 V (vs Ag/AgCl) (0.8 V)	1.0 M KOH	80.1	360	27
PPrGO-1				59.2	266	
PPrGO-3				55.9	252	
PPrGO-4				52.4	236	
CAP-1	1	0 V ~ 1.0 V (vs SCE) (1.0 V)	2.0 M KCl	66.7	240	28
CAP-2				22.2	80	
PAQTA	1 10	0.2 V ~ 0.8 V (vs Ag/AgCl) (0.8 V)	0.5 M H <sub>2</sub> SO <sub>4</sub>	96	576	29
				68.3	410	
TPA-COFs	0.1 5	0 V ~ 1.0 V (vs SCE) (1.0 V)	1.0 M H <sub>2</sub> SO <sub>4</sub>	73.1	263	30
				45.3	163	
TNNs-550	0.2 10	-0.2 V ~ 0.8 V (vs Ag/AgCl) (1.0 V)	1.0 M H <sub>2</sub> SO <sub>4</sub>	82.8	298	31
				48.1	173	
PYBDA	0.5	-0.2 V ~ 0.6 V (vs SCE) (0.8 V)	2.0 M H <sub>2</sub> SO <sub>4</sub>	101.3	456	32
POPM-TFP	0.5 8	0 V ~ 0.5 V (vs Hg/HgO) (0.5 V)	2.0 M KOH	24.7	178	33
				10.7	77	
TPPDA-TPTPE COF	2	-0.92 V ~ 0.18 V (vs Hg/HgO) (1.0 V)	1.0 M KOH	72.4	237	34
TPPDA-TPPy COF				57.7	189	
Pyrene-CTF-10	0.5	-1.0 V ~ 0 V (vs Hg/HgO) (1.0 V)	1.0 M KOH	105.6	380	35
Pyrene-CTF-20				138.9	500	
CC-DAQ-CMP	1 10	-1.2 V ~ -0.5 V (vs SCE) (0.7 V)	6.0 M KOH	35.8	184	36
				17.2	88	
DAAQ-COFs/GA	1 20 70	-0.5 V ~ 0.5 V (vs SCE) (1.0 V)	1.0 M H <sub>2</sub> SO <sub>4</sub>	105	378	37
				89.4	322	
				85.6	308	
TAT-CMP-1	1 10	-1.0 V ~ 0 V (vs Hg/HgO) (1.0 V)	1.0 M Na <sub>2</sub> SO <sub>4</sub>	39.2	141	38
				27.5	99	
TAT-CMP-2	1 10	(1.0 V)		50.8	183	
				38.1	137	
PDC-MA-COF	1 10	0 V ~ 0.6 V (vs Ag/AgCl) (0.6 V)	6.0 M KOH	37.2	335	39
				27.6	248	

Table S3. Comparison of charge capacity (mAh g<sup>-1</sup>), and capacitance (F g<sup>-1</sup>) between PI-Fiber and materials in previously reported literature. Capacitance values represented are all calculated by following equations; Capacitance (F g<sup>-1</sup>) =  $\frac{\text{Charge capacity (A s g}^{-1}\text{)}}{\text{Applied potential (V)}}$ .

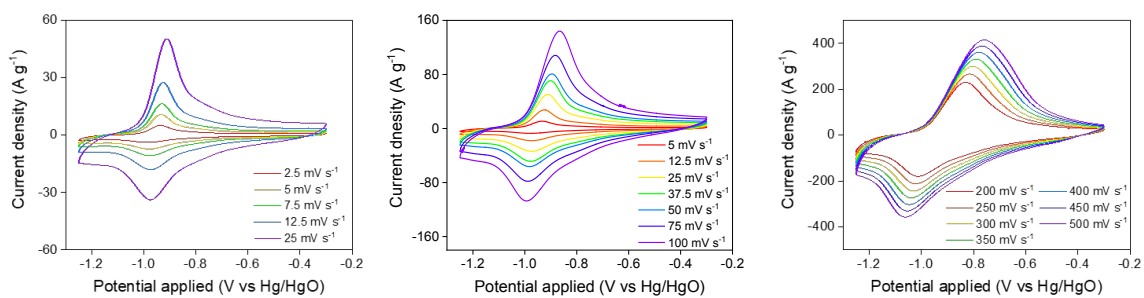
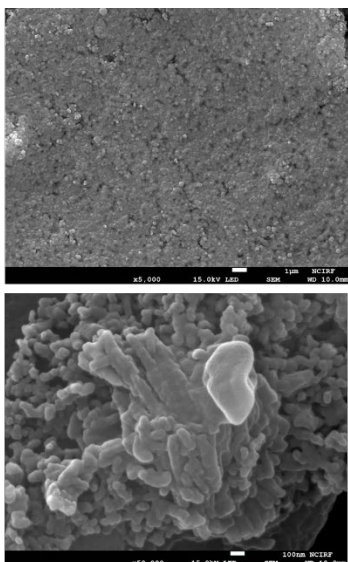


Fig. S29. CV curves of cycled electrode at different scan rates (2.5–500 mV s<sup>-1</sup>). All other experimental conditions were the same as in Fig. S23.

No cycling



500 times cycling

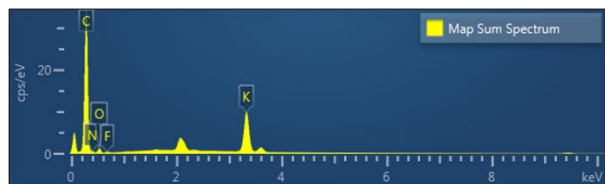
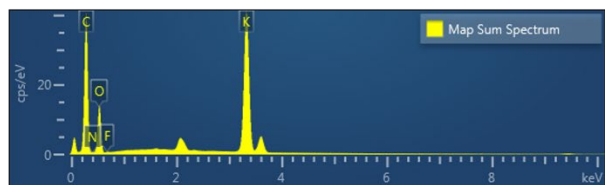
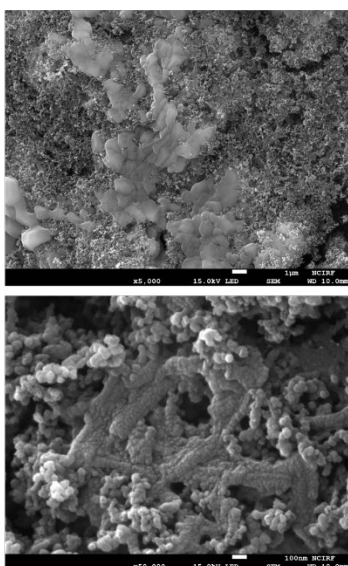


Fig. S30. SEM images and EDS analysis of electrodes before and after cycling.

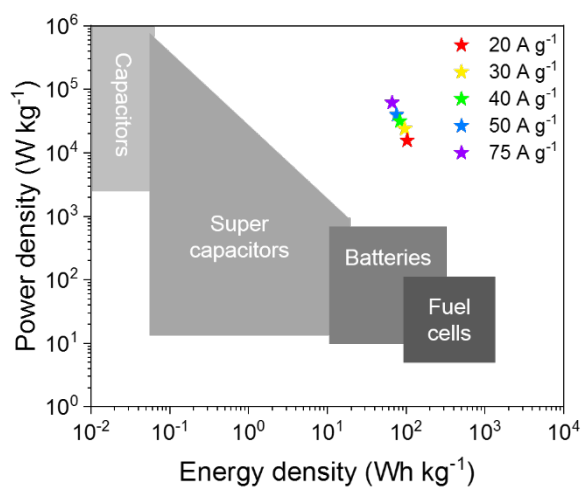


Fig. S31. Ragone plot of AC//PI-Fiber. Specific energy densities and power densities were calculated by using the mass of the active material, not a whole device.

Current density (A g <sup>-1</sup> )	The energy density (Wh kg <sup>-1</sup> )	Power density (kW kg <sup>-1</sup> )
20	103.2	15.7
30	96.0	23.8
40	83.3	31.6
50	75.9	39.6
75	66.3	61.2

Table S4. The electrochemical performance of AC//PI-Fiber. All values were calculated as described in Fig. S29.

## References

- 1 K. Kanakarajan, A. W. Czarnik, *J. Org. Chem.* **1986**, *51*, 5241.
- 2 T. Aoki, H. Sakai, K. Ohkubo, T. Sakanoue, T. Takenobu, S. Fukuzumi, T. Hasobe, *Chem. Sci.* **2015**, *6*, 1498.
- 3 A. J. Fatiadi, W. F. Sager, *Org. Synth.* **1962**, *42*, 90.
- 4 J. T. Rademacher, K. Kanakarajan, A. W. Czarnik, *Synthesis* **1994**, *04*, 378.
- 5 X. Li, Q. Gao, J. Aneesh, H.-S. Xu, Z. Chen, W. Tang, C. Liu, X. Shi, K. V. Adarsh, Y. Lu, K. P. Loh, *Chem. Mater.* **2018**, *30*, 5743.
- 6 Z. Yang, J. Liu, Y. Li, G. Zhang, G. Xing, L. Chen, *Angew. Chem. Int. Ed.* **2021**, *60*, 20754.
- 7 Y. Yang, P. Zhang, L. Hao, P. Cheng, Y. Chen, Z. Zhang, *Angew. Chem. Int. Ed.* **2021**, *133*, 2.
- 8 J. C. Russell, V. A. Posey, J. Gray, R. May, D. A. Reed, H. Zhang, L. E. Marbella, M. L. Steigerwald, Y. Yang, X. Roy, C. Nuckolls, S. R. Peurifoy, *Nat. Mater.* **2021**, *20*, 1136.
- 9 M. Li, J. Liu, Y. Li, G. Xing, X. Yu, C. Peng, L. Chen, *CCS Chem.* **2021**, *3*, 696.
- 10 A. F. M. El-Mahdy, Y. H. Hung, T. H. Mansoure, H. H. Yu, T. Chen, S. W. Kuo, *Chem. Asian. J.* **2019**, *14*, 1429.
- 11 S. R. Peurifoy, J. C. Russell, T. J. Sisto, Y. Yang, X. Roy, C. Nuckolls, *J. Am. Chem. Soc.* **2018**, *140*, 10960.
- 12 S. Chandra, D. Roy Chowdhury, M. Addicoat, T. Heine, A. Paul, R. Banerjee, *Chem. Mater.* **2017**, *29*, 2074.
- 13 P. Bhanja, S. K. Das, K. Bhunia, D. Pradhan, T. Hayashi, Y. Hijikata, S. Irle, A. Bhaumik, *ACS Sustainable Chem. Eng.* **2017**, *6*, 202.
- 14 P. Bhanja, K. Bhunia, S. K. Das, D. Pradhan, R. Kimura, Y. Hijikata, S. Irle, A. Bhaumik, *ChemSusChem* **2017**, *10*, 921.
- 15 C. R. DeBlase, K. E. Silberstein, T. T. Truong, H. D. Abruna, W. R. Dichtel, *J. Am. Chem. Soc.* **2013**, *135*, 16821.
- 16 S. Vargheese, R. T. R. Kumar, Y. Haldorai, *Mater. Lett.* **2019**, *249*, 53.
- 17 R. Xue, Y.-P. Zheng, D.-Q. Qian, D.-Y. Xu, Y.-S. Liu, S.-L. Huang, G.-Y. Yang, *Mater. Lett.* **2021**, *308*, 131229.
- 18 R. Vinodh, C. V. V. Muralee Gopi, Z. Yang, C. Deviprasath, R. Atchudan, V. Raman, M. Yi, H.-J. Kim, *J. Energy Storage* **2020**, *28*, 101283.

- 19 Y. Zhang, L. Cheng, L. Zhang, D. Yang, C. Du, L. Wan, J. Chen, M. Xie, *J. Energy Storage* **2021**, *34*, 101786.
- 20 X. Kong, S. Zhou, M. Strømme, C. Xu, *Carbon* **2021**, *171*, 248.
- 21 A. Roy, S. Mondal, A. Halder, A. Banerjee, D. Ghoshal, A. Paul, S. Malik, *Eur. Polym. J.* **2017**, *93*, 448.
- 22 Y. Zhang, B. Zhang, L. Chen, T. Wang, M. Di, F. Jiang, X. Xu, S. Qiao, *J. Colloid. Interface. Sci.* **2022**, *606*, 1534.
- 23 J. Chen, C. Du, Y. Zhang, W. Wei, L. Wan, M. Xie, Z. Tian, *Polymer* **2019**, *162*, 43-49.
- 24 M. G. Mohamed, X. Zhang, T. H. Mansoure, A. F. M. El-Mahdy, C.-F. Huang, M. Danko, Z. Xin, S.-W. Kuo, *Polymer* **2020**, *205*, 122857.
- 25 S. K. Das, K. Bhunia, A. Mallick, A. Pradhan, D. Pradhan, A. Bhaumik, *Microporous Mesoporous Mater.* **2018**, *266*, 109.
- 26 Y. Gao, C. Zhi, P. Cui, K. A. I. Zhang, L.-P. Lv, Y. Wang, *Chem. Eng. J.* **2020**, *400*, 124071.
- 27 M. Sajjad, R. Tao, K. Kang, S. Luo, L. Qiu, *ACS Appl. Energy Mater.* **2021**, *4*, 828.
- 28 W. Liu, M. Ulaganathan, I. Abdelwahab, X. Luo, Z. Chen, S. J. Rong Tan, X. Wang, Y. Liu, D. Geng, Y. Bao, J. Chen, K. P. Loh, *ACS Nano* **2018**, *12*, 852.
- 29 Y. Liao, H. Wang, M. Zhu, A. Thomas, *Adv. Mater.* **2018**, *30*, e1705710.
- 30 S. Xiong, J. Liu, Y. Wang, X. Wang, J. Chu, R. Zhang, M. Gong, B. Wu, *J. Appl. Polym. Sci.* **2021**, *139*, e51510
- 31 L. Hao, B. Luo, X. Li, M. Jin, Y. Fang, Z. Tang, Y. Jia, M. Liang, A. Thomas, J. Yang, L. Zhi, *Energy Environ. Sci.* **2012**, *5*, 9747.
- 32 S. Bandyopadhyay, C. Singh, P. Jash, M. D. W. Hussain, A. Paul, A. Patra, *Chem. Commun.* **2018**, *54*, 6796.
- 33 L. Xu, R. Liu, F. Wang, S. Yan, X. Shi, J. Yang, *RSC Adv.* **2019**, *9*, 1586.
- 34 A. F. M. El-Mahdy, M. G. Mohamed, T. H. Mansoure, H.-H. Yu, T. Chen, S.-W. Kuo, *Chem. Commun.* **2019**, *55*, 14890.
- 35 M. G. Mohamed, A. F. M. El-Mahdy, Y. Takashi, S.-W. Kuo, *New J. Chem.* **2020**, *44*, 8241.
- 36 B. Luo, Y. Chen, Y. Zhang, J. Huo, *New J. Chem.* **2021**, *45*, 17278.
- 37 N. An, Z. Guo, J. Xin, Y. He, K. Xie, D. Sun, X. Dong, Z. Hu, *J. Mater. Chem. A* **2021**, *9*, 16824.
- 38 X.-C. Li, Y. Zhang, C.-Y. Wang, Y. Wan, W.-Y. Lai, H. Pang, W. Huang, *Chem. Sci.* **2017**, *8*, 2959.

39 L. Li, F. Lu, R. Xue, B. Ma, Q. Li, N. Wu, H. Liu, W. Yao, H. Guo, W. Yang, *ACS Appl. Mater. Interfaces* **2019**, *11*, 26355.